Cryogenics 63 (2014) 17–24

Contents lists available at ScienceDirect

Cryogenics

journal homepage: www.elsevier.com/locate/cryogenics

Longitudinal inhomogeneity of DC current transport properties in Gd-system HTS tapes – Statistical approach for system design

T. Nakamura [a,*], Y. Takamura [a], N. Amemiya [a], K. Nakao [b], T. Izumi [b]

[a] Graduate School of Engineering, Kyoto University, 1 Kyoto-daigaku-katsura, Nishikyo-ku, Kyoto 615-8510, Japan
[b] Superconductivity Research Laboratory, ISTEC, 1-10-13 Shinonome, Koto-ku, Tokyo 135-0062, Japan

ARTICLE INFO

Article history:
Received 1 September 2013
Received in revised form 4 May 2014
Accepted 6 May 2014
Available online 20 May 2014

Keywords:
GdBCO-coated conductor
Inhomogeneous current transport
Statistical method
TapeStar™
Pancake coil

ABSTRACT

In this paper, we studied the DC current transport properties of GdBCO-coated conductors, including the longitudinal distribution of critical current. Inhomogeneity of the local critical current was firstly measured by means of TapeStar™ at 77 K, and then characterized based on a statistical method. Current transport properties were also measured for different positions and/or distances of potential taps using a four-probe method. It was shown that the longitudinal inhomogeneity of the conductor was described by use of a simplified percolation depinning model that takes account of Gaussian distribution. We further distinguished the above-mentioned inhomogeneity between statistical distribution and random failure. Influence of the aforementioned statistically distributed current transport properties on the magnet performance was also elucidated for simple pancake coils. This information is important as it provides guidance for practical system design.

© 2014 Elsevier Ltd. All rights reserved.

1. Introduction

RE-system High Temperature Superconductor (HTS) tapes possess excellent current transport property at higher temperature compared to that of Bi-system HTS ones, and also high tolerance against mechanical stress. Therefore, R&Ds applied to the tapes have energetically been carried out worldwide. Especially, power transmission cables [1,2] and high field magnets [3,4] are the major field of such applications.

On the other hand, RE-system HTS tapes are also called 'coated conductors', which apply the thin film production technology. And then, even tape-shape HTS wires are realized by means of artistic IBAD method invented in Japan [5], there exist various obstacles for the practical utilization of such wires. For instance, the first author's group studied the relationship between stress vs. strain properties obtained from uniaxial tensile test and critical current in Y-system HTS wires developed for the magnetic energy storage coils. In their study, although the elastic limit of such tapes is more than 1 GPa, the interface in between the superconducting layer and the buffer layer is weaker against the shear stress, are reported that the potential danger of delamination for the stress [6] (At the same international conference, Ekin et al. has also reported such problems from the different experiment [7]). In these days, the above-mentioned problems are getting a great deal of attention, various kinds of studies for its prevention measure are underway, e.g., windings technology [8]. There have also been pointed out experimentally and analytically that the riskiness of the interlayer becoming large thermal resistance [9,10].

In order to accelerate the practical application of the RE-system wires by overcoming the aforementioned obstacles, mature production technology of such wires are mandatory to be realized. Especially, with respect to the superconducting property along the longitudinal direction of the wires, high homogeneity (yield) is crucial as for the establishment of a status as industrial materials. Due to the above-mentioned specific production process, however, high precision and wide range control over the complicated parameters should be taken for the crystal growth, in order to realize the tape production technology along the longitudinal direction with high homogeneity. Therefore, it is significant to deal with the longitudinal inhomogeneity of current transport properties in a systematic and quantitative way for the setting of a target of an improvement in the tape property. Moreover, if it is revealed that how much influence such inhomogeneity gives onto the characteristics of superconductor apparatuses, it is expected to realize the system design that allows the inhomogeneity to some extent.

In this study, our purpose is to investigate the longitudinal inhomogeneity of current transport properties in GdBCO-system tape conductor from the viewpoint of statistical approach. Longitudinal

* Corresponding author. Address: Department of Electrical Engineering, Graduate School of Engineering, Kyoto University, 1 Kyoto-daigaku-katsura, Nishikyo-ku, Kyoto 615-8510, Japan. Tel.: +81 75 383 2221; fax: +81 75 383 2224.
E-mail address: tk_naka@kuee.kyoto-u.ac.jp (T. Nakamura).

http://dx.doi.org/10.1016/j.cryogenics.2014.05.004
0011-2275/© 2014 Elsevier Ltd. All rights reserved.

distribution of local critical current density in the subject sample is firstly evaluated by means of TapeStar™. And then, the statistical consideration is given to the estimated current transport property obtained from summation of the above result, by comparing with that from a typical DC four-probe method. Furthermore, applying the longitudinally inhomogeneous current transport properties to a simple pancake coil, analytical study is executed on its influence.

Note that our study is valid only for the macroscopic physics quantity. In the sense that we obtain integrated information from the mesoscopical dimension (spatial resolution dominated roughly by the elemental interaction between quantized flux lattice and flux pinning center), we cannot yet give the index for the uniform material production. However, combining a TapeStar™ with a four-probe method is likely to generate a base of the index for its homogeneity in terms of its application.

2. Fundamental concept of inhomogeneous current transport property evaluation

2.1. Current transport property of HTS apparatuses

On designing Low Temperature Superconductor (LTS) apparatuses, the operation current is generally determined based on the critical current of its short samples, which is dominated by the maximum magnetic field that such samples will experience. This is because so-called quench propagation velocity is extremely high in the LTS tapes, and even small region of the normal conducting (or dissipative flux-flow) state trigger the overall and catastrophic quench phenomenon [11,12].

On the other hand, the above-mentioned propagation velocity is quite low in the HTS apparatuses, which is operated at temperature higher than 20 K, and the locally generated heat region will stay there (hot-spot) [13]. This fact loses generality of the aforementioned design concept, and derives necessity of description for not only the critical current itself but also the accurate electric field vs. current density properties in the HTS tapes [14–16]. This also demands the precise estimation of the heat generation that widely distribute in the apparatuses [17].

Fig. 1 shows basic concept of the aforementioned current transport property evaluation (in this figure, it is assumed that the critical current distribution for lateral direction at ith component of the tape is contained in $I_{c,l}$. It is also necessary to extend this method for consideration of the magnetizing current due to the electromagnetic induction as well as its relaxation). In the upper figure, temperature, T_i, magnetic field vector, $\boldsymbol{H}_i$, and mechanical strain, ε_i, at the local point, x_i, are mapped on the line element, which is changed depending upon the practical shapes of the applications such as coil and cable, and then the total voltage is calculated by summing up such local one (lower figure of Fig. 1). Kiss's group has proposed quantitative formulation of E_i vs. I curve based upon so-called percolation transition model [18], and then this model has successfully introduced to the expression of the current transport characteristics analyses for various kinds of applications [14–16] (details will be explained later).

The first author's group has also performed the analytical study with the use of the above-mentioned model for HTS coils [19–25] and HTS cables [26,27]. In this paper, variables T_i and ε_i are not subjected to the consideration.

2.2. Expression of longitudinal inhomogeneity of current transport property [28]

In this section, in addition to the evaluation method of current transport property described in 2.1, the evaluation method for its longitudinal inhomogeneity is explained. It should be noted that the percolation transition model dealt in the previous section [14–16] is also formulated based upon the pinning force inhomogeneity under mesoscopic scale. That is, the analytical expression can be obtained by convolution of the local electric field with the pinning force distribution in the above-mentioned scale (see the references [14–16] for the details).

On the other hand, the longitudinal inhomogeneity described in this section is macroscopically affected origins, and then such inhomogeneity will directly influence the (observable) current transport properties. Then, the longitudinal inhomogeneity assuming the statistical distribution of the critical current ($I_{c,l}$), which is defined by the electric field criterion, is investigated. It should be noted that if the electric field criterion for the definition of $I_{c,l}$ is comparable to that for the value of V_t (Fig. 1), local heat generation dominates the overall characteristics in the tape. And this may cause the failure of the aforementioned statistical study. Therefore, the former should be set adequately lower than the latter.

Fig. 2 shows the schematic diagram of probability density function (the Gaussian distribution) giving longitudinal distribution of the value $I_{c,l}$. Eq. (1) describes the probability density function P ($I_{c,l}$) of the Gaussian distribution.

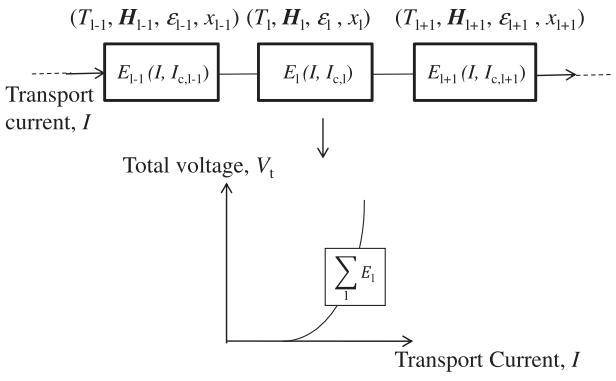

Fig. 1. Schematic illustration of the calculation of current transport properties in HTS apparatuses. Local electric field (E_l) as a function of temperature (T_l), magnetic field vector ($\boldsymbol{H}_l$) and strain (ε_l), which is mapped from actual geometrical shape of the apparatuses such as cables and magnets (upper figure), are summed to calculate total voltage (V_t) (lower figure).

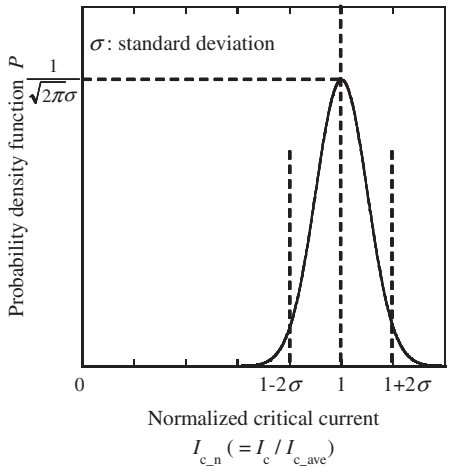

Fig. 2. Schematic diagram of the probability density function of the inhomogeneity of normalized critical current along the longitudinal direction of the HTS tape conductors (I_{c_ave}: mean value of critical current distribution; σ: standard deviation).

$$P(I_{c,l}) = \frac{1}{\sqrt{2\pi\sigma^2}} \exp\left(-\frac{I_{c,l} - I_{c,ave}}{\sqrt{2}\sigma}\right)^2 \quad (1)$$

Here I_{c_ave} denotes the average value of the critical current distribution, and σ gives its standard deviation. When the value $I_{c,l}$ in Fig. 1 follows the Gaussian distribution, it is to be called "the statistical inhomogeneity" and when not follows, "the accidental inhomogeneity". The both should be distinguished.

3. Evaluation result and discussion for current transport properties

3.1. Specification of subject sample

Table 1 shows the specification of the GdBCO sample for the measurement subject (silver is utilized as the stabilization layer). The sample at the length of 2400 mm is taken out from the original long length tape material (10 mm wide) produced by the IBAD/PLD process, and then by cutting with laser beam, the tape is narrowed by 5 mm in width as a sample to measure. As far as the sample is from the same rod, the average critical current value in the tape (10 mm wide) is approximately twice as high as the one in the narrowed tape. It is proved that there is no attended deterioration of the superconducting characteristic by the cutting.

3.2. Local critical current distribution by TapeStar™

The local critical current distribution ($I_{c,1}$) is firstly measured by means of TapeStar™ at 77 K. The value $I_{c,l}$ is measured based on so-called induction method, in which it is evaluated approximately every 0.5 mm on the tape along the longitudinal direction (external applied magnetic field is 10∼40 mT; for the detailed measurement principle of the TapeStar™, see the references [29,30]). Since there are two kinds of induced current information, i.e., intra-grain and inter-grain current paths, in the induction method, and the inter-grain character is dominant from the perspective of spatial resolution of this measurement. Furthermore, the electric field criteria to define $I_{c,1}$ is approximately 1 μV m^{-1}, which is smaller by two orders in the comparison with the normal value (100 μV m^{-1}) used in the current transport method.

Fig. 3 shows the experimental result of the $I_{c,1}$ obtained over the length of 2400 mm. The average value of $I_{c,1}$ is approximately 110 A according to the graph. On the other hand, there exist roughly two kinds of inhomogeneity in the value of $I_{c,l}$. The one is the inhomogeneity that varies regarding the average $I_{c,l}$ value like a fluctuation, which period is approx. 200 mm. The other is the one which varies spike-like and is mainly lower than the average. This inhomogeneity has less correlation with adjacent values. In this paper, for further discussion, the regions with the value $I_{c,l}$, which standard deviation is considerably lower than 2σ, are marked by circles with alphabetical symbols (A), (B) and (C).

Fig. 4 shows the histogram of the local critical current $I_{c,l}$ obtained from Fig. 3. As can be seen in the figure, the curves seem to follow symmetrical distribution. Fitted by means of the Gaussian distribution (Eq. (1)), we can see it fits in the range of σ between 0.04 and 0.05. Namely, although the longitudinal distribution of the value $I_{c,l}$ in Fig. 3 looks random at the first glance, such distribution in almost all the regions actually coincide the Gaussian distribution, and therefore meet the expectations of statistical approach (statistical inhomogeneity in 2.2). Especially, it is interesting to know the fact that even though the value $I_{c,1}$ fluctuates within the range of approx. every 200 mm (Fig. 3), it follows the Gaussian distribution. On the other hand, points (A), (B) and (C) are considered as the candidates for the accidental inhomogeneity. We talk about later whether these three points come from the characteristic of the accidental inhomogeneity or from simply the statistical inhomogeneity with large standard deviation.

Table 1
Specifications of the GdBCO tape sample.

Process	IBAD/PLD
Stabilization layer	Silver
Thickness of SC layer	∼0.5 μm
Width	5.0 mm
Length subjected in this study	2400 mm

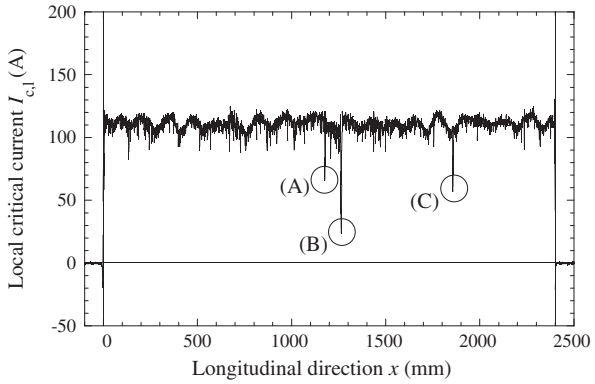

Fig. 3. Experimental result of the local critical current ($I_{c,l}$) in the GdBCO sample at 77 K obtained using TapeStar™. Distinctly damaged regions with respect to the local critical currents are marked by circles with alphabetical symbols, i.e., (A), (B) and (C).

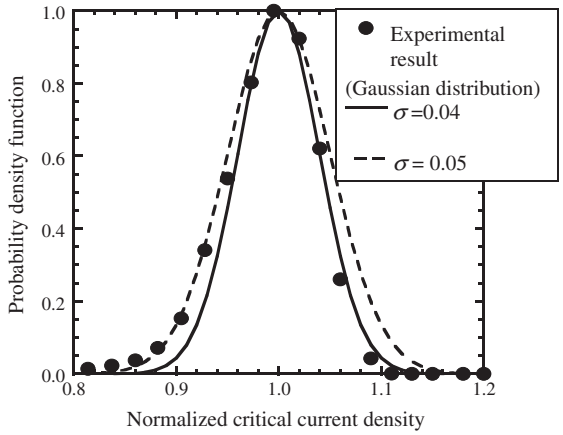

Fig. 4. Histogram of the local critical current ($I_{c,l}$) obtained from Fig. 3. Solid circles are the experimental data (Fig. 3) and curves are the Gaussian distribution (solid curve: σ = 0.04; broken curve: σ = 0.05).

3.3. Evaluation of current transport properties obtained from four-probe method

With respect to the identical sample in 3.1, the four-probe measurements of the current transport properties are carried out. Fig. 5 shows the potential taps arrangement and the corresponding taps numbers (the distance between taps is set to be 300 mm except both the ends.)

Fig. 6 shows the experimental results of the current transport properties obtained from the measurement between tap numbers ⟨1⟩ through ⟨4⟩. From the graph, it is clear that each *E–I* property measured between taps at four different points mostly coincide one another; the corresponding critical current is 135 A at the

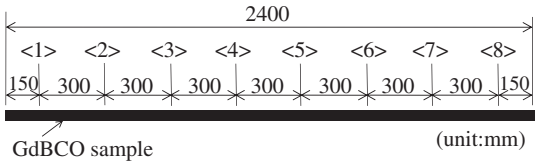

Fig. 5. Potential taps arrangement and tap numbers for four-probe measurement of current transport properties.

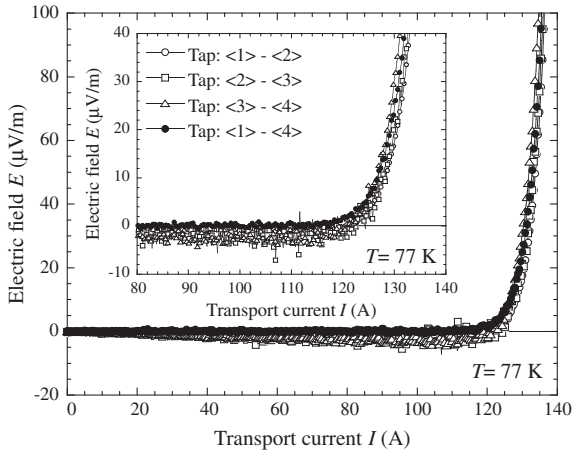

Fig. 6. Experimental results of current transport properties in the GdBCO sample (inset: enlarged view of the area around the take-off of the curve; for tap number, see Fig. 5).

electric field criterion of 100 μV m^{-1}, which is larger than the average value obtained from the TapeStar™ (110 A at the value 1 μV m^{-1} of electric field criterion). The similar property can be observed at the enlarged view of the area around the take-off of the curve (see the inset). Thus it is possibly suggested that these properties coincide with the similar statistical distribution within the range of the present measurements (Fig. 4); even though there exists local inhomogeneity as Fig. 3, they coincide each other no dependence of measurement points. In other words, we assume that there is no such an area as the accidental inhomogeneity regions between taps ⟨1⟩ and ⟨4⟩, and the characteristic degradation point (A) is also considered to belong to the statistical inhomogeneity.

For the further examination, we derive the analytical expression of the current transport property using the result of TapeStar™ (Fig. 3), and then the obtained results are compared with Fig. 6. In order to evaluate the current transport property from Fig. 3, however, the formulation to the generated electric field needs to be given in the flux-flow state. We, in our previous analyses, have used the most reliable formulation of Kiss's percolation transition model [14–16]. However (even though to examine with the direct use of the above-mentioned model is necessary), this model does not serve the purpose of the study; because the consideration should be taken into the influence on all the crucial parameters it holds, upon the discussion the longitudinal inhomogeneity. Thus we are to discuss, assuming that the evaluation formula is given by a simplified percolation transition model as follows,

$$V_l(x_l, I) = K(I - I_{c,l}(x_l))^{n_p} \Delta x_l \tag{2}$$

where $I_{c,l}(x_l)$ denotes the local critical current obtained from the TapeStar™ (Fig. 3). K is the coefficient with the dimension of resistance per unit length, and n_p is the power index. Δx_l ($= x_l - x_{l-1}$) is the space between adjacent taps that defines the value $I_{c,l}(x_l)$, with a slight deference of 0.5 mm depending on the measured points. Note that Eq. (2) formally coincides so-called Generalized critical state

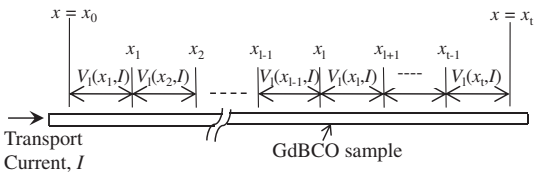

Fig. 7. Schematic explanation for the summation of local flux-flow voltage, V_l. Total tape length is defined as x_t–x_0 and total voltage is denoted as V_t.

model [31]. Furthermore, the overall tape voltage V_t is calculated on the basis of the following equation led from Fig. 7.

$$V_t(I) = \sum_{i=1}^{t} V_l(x_l, I) \tag{3}$$

We examine the coincidence between the experimental result of TapeStar™ (Fig. 3) and that of the four-probe method (Fig. 6), assuming K and n_p as fitting parameters in Eqs. (2) and (3). It should be noted again that analysis on the basis of Eq. (3) is considered to be valid at least around the take-off of the curve, from the perspective that while V_l is below 1 μV m^{-1}, V_t is approx. within 10–100 μV m^{-1}. The current sharing to the silver stabilization layer is neglected in this study.

Fig. 8 shows the evaluation result for taps ⟨1⟩–⟨2⟩. As it is clear from the diagram, the results obtained using the TapeStar™ and that of the four-probe method coincide with each other. The same agreement is also obtained for all tap combinations between taps ⟨1⟩ and ⟨4⟩. It is apparent from these results that the current transport properties between taps ⟨1⟩ and ⟨4⟩ are dominated by the Gaussian distribution. Note that the power index n_p at this occasion is identical for all the data, i.e., $n_p = 8$. The physical meaning of the power index in this case is now under investigation (measuring the magnetic field dependency of E–I property for short sample, we get almost the same power index value as that of so-called percolation transition point [14–18]).

However, in the similar comparison for taps ⟨1⟩–⟨8⟩, as Fig. 9 shows, the both do not coincide at all. The same results are obtained in another comparison including taps ⟨4⟩–⟨8⟩. That suggests the current transport properties in the aforementioned section do not agree with the Gaussian distribution. Fig. 3 says that the characteristic degradation points (B) and (C) exist between taps ⟨4⟩–⟨8⟩. It is assumed that the current transport properties are made lower at these points where the characteristics of accidental

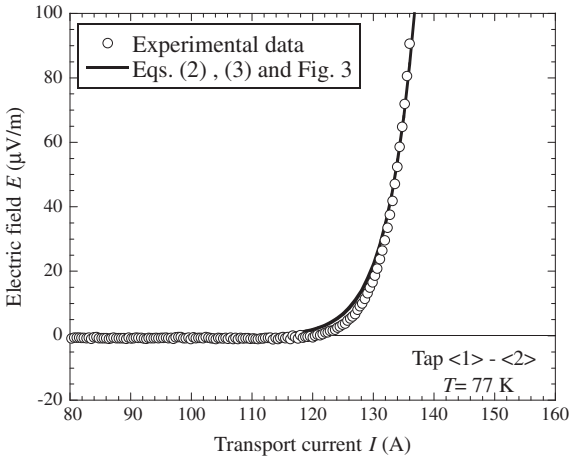

Fig. 8. Comparison between Eqs. (2) and (3) (Fig. 3) and Fig. 6 for taps ⟨1⟩–⟨2⟩. The same agreements are also obtained for all tap combinations between tap ⟨1⟩ and ⟨4⟩. Statistical inhomogeneity is dominant in this curve.

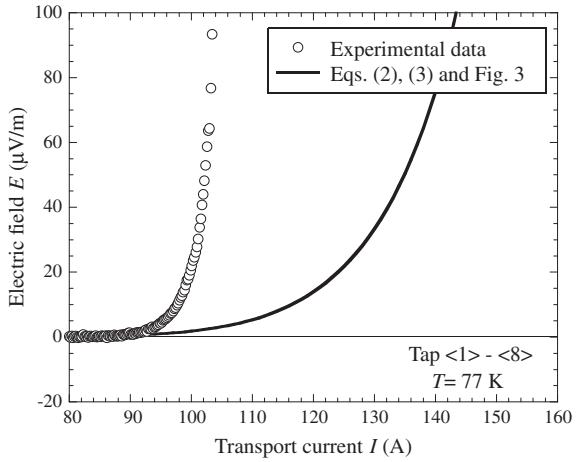

Fig. 9. Comparison between Eqs. (2) and (3) (Fig. 3) and Fig. 6 for taps ⟨1⟩–⟨8⟩. Stochastic inhomogeneity (random failure) is dominant in this curve.

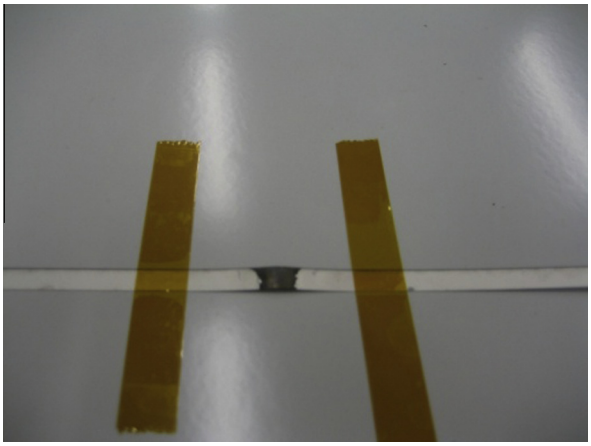

Fig. 10. Photograph of the burn-out point ((C) in Fig. 3) at the measurement process of Fig. 9.

inhomogeneity are brought into and end up overwhelming that of the statistical inhomogeneity. As a typical event the accidental inhomogeneity holds, even though the electric field criterion is approx. 100 $\mu V\,m^{-1}$ during the experiment in Fig. 9, the tapes are burnt out. The burn-out point is not on point (B), the lowest critical current, but (C) (see Fig. 3). That is, at the points of the accidental inhomogeneity, the hot-spot like local burn-out occurs (see Fig. 10), and such event is dominated by the stochastic process that makes the prediction of burn-out point difficult.

From the study, there exist two kinds of inhomogeneity, i.e., the statistical inhomogeneity and the accidental inhomogeneity, with respect to the longitudinal distribution of the critical current in the sample subject. Further improvement of the production technology is necessary as for the statistical inhomogeneity; on the other hand, some tolerance to design them may be acceptable. However, we understand the accidental inhomogeneity must be preferentially removed.

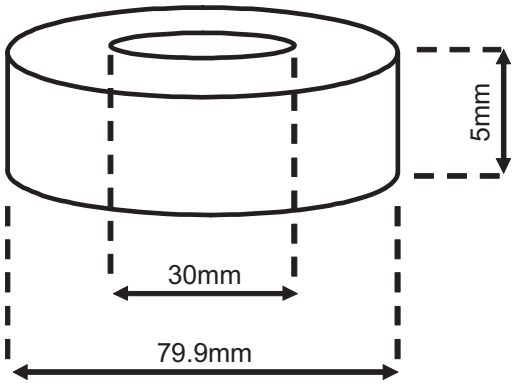

Fig. 11. Schematic diagram of the simple pancake coil for the analysis of inhomogeneous current transport properties (turn number: 100). The central magnetic field is designed for 0.123 T at 100 A.

4. Inhomogeneous current transport properties of pancake coil

4.1. Analysis method

In the previous sections, we clearly understand the relationship between the longitudinal inhomogeneity of the local critical current in tapes and the corresponding current transport properties. In this chapter, we analyze the influence of the aforementioned inhomogeneity on the current transport performance of a simple pancake coil, as specific equipment. Note that here we are to deal with statistical inhomogeneity only; not unpredictable accidental inhomogeneity. As this research advances, the homogeneous target value along the longitudinal direction gets clearer for the tolerant system design. Moreover, the permissible inhomogeneity from the coil properties is more obvious and is to accelerate a system development.

Fig. 11 shows the schematic diagram of the simple pancake coil for the analysis subject. The inner diameter, the outer diameter and the height of the coil are, correspondingly, 30.0 mm, 79.9 mm and 5.0 mm. The central magnetic field is designed for 0.123 T at the excitation current of 100 A. Concerning the coil in Fig. 11, on the basis of the electromagnetic field analysis, setting the spatial distributions of the magnetic field vector for the forced current in a database of all meshes in advance. And then, the dissipative characteristics of the coil are analyzed by means of the method in Section 2 as follows.

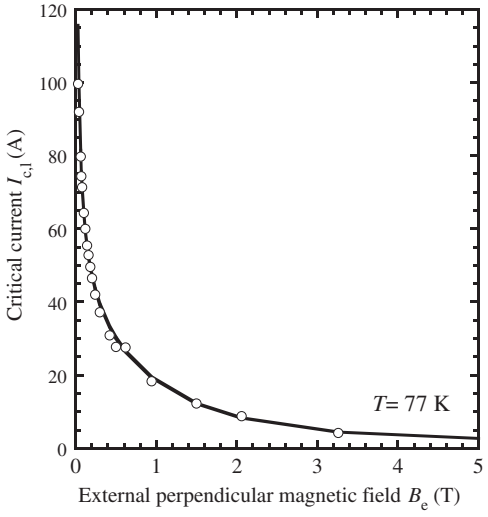

Fig. 12. External magnetic field dependence of critical current in GdBCO short sample at 77 K. The magnetic field is applied perpendicular to the broad surface of the tape. Symbols (circles) are the experimental data and the curve is the fitted property using Eq. (4).

Fig. 12 shows the external magnetic field dependence of critical current in GdBCO tapes (circles). The magnetic field (B_e) is applied always perpendicular to the broad surface of the tape. That is, it is known that the critical current is dominated by the perpendicular component of the applied magnetic field. On the assumption that the following Eq. (4) led from the Mawataris' report [32], we successfully get the fitted property curve as shown in Fig. 12.

$$I_{c,l}(B_e) = \varepsilon K_1 B_e^{-\alpha} + (1-\varepsilon)K_2 \exp^{-B_e} \quad (4)$$

Here, the first term dominates the lower magnetic field property and the second describes the higher magnetic field property. K_1 and K_2 are the respective coefficients in the above-mentioned equation, and ε is the weight coefficient in each section.

First, the local voltage V_l at each point that possesses local critical current of $I_{c,l}$ inside the coil is calculated using Eq. (2). By dividing the maximum local voltage among the above-mentioned V_ls by the element division length, the maximum local electric field $E_{l,m}$ is obtained. All the V_ls in the coil are also summed (Eq. (3)), and that makes a total (end-to-end) voltage V_t. Then, multiplying the aforementioned voltage V_t by the transport current leads to the total heat generation W_t. Moreover, concerning all the elements inside the coil, the statistical inhomogeneity is given by use of random numbers for $I_{c,l}$ according to the standard deviation σ in Eq. (1). Such calculations are repeated 100 times for above-mentioned $E_{l,m}$ and W_t in order to realize the statistical process. Note that to examine both $E_{l,m}$ and W_t are important for the control of the hot-spot and the total heat generation of the coil, respectively [21–25].

4.2. Analysis results and discussion

Fig. 13 shows the analysis results of the electric field for total length of the coil (E_t), at different values of the transport current (I_t) and the standard deviation (σ). E_t is obtained from V_t (Eq. (3); the expected values of the statistical process are utilized) divided by the total length of the tape. As can be seen in the figure, E_t, especially at the lower electric field region, drastically increases when σ is more than 0.04. For example, on the condition that the transport current I is to be 70 A, the value E_t at $\sigma = 0$ is different more than by 2 orders than that at $\sigma = 0.10$. From this point of view, we understand the longitudinal inhomogeneity of the critical current in the tape deeply affect the current transport property of the coil, even if such property is evaluated by the expected value in the statistical process.

Fig. 14 shows the analysis results of (a) the maximum local electric field ($E_{l,m}$) and (b) the total heat generation (W_t) in the coil. By comparing Fig. 13 with Fig. 14(a), we observe that $E_{l,m}$ is much larger by orders than E_t and that the longitudinal inhomogeneity will become origin of the severe hot-spots. The bigger σ gets, the more both $E_{l,m}$ and W_t increase, that is, the longitudinal inhomogeneity is greatly influential as far as it is concerned. Furthermore, looking at the error bars for the event number 100, we understand that the bigger the inhomogeneity (σ) gets, the more seriously $E_{l,m}$ is affected, but not so much for W_t. Namely, as the statistical inhomogeneity increases, it is obvious that the uniqueness of $E_{l,m}$ at the lower electric field gets damaged. Thus, it is not sufficient to discuss $E_{l,m}$ only from the perspective of the expected values, but necessary to do so with a wide view to error bars. In some cases, it may also be required to impose further pessimistic restriction on $E_{l,m}$. It is noted that the similar results are reported concerning the coil for magnetic energy storage [33]. To be exact, we have to consider the effect of the current sharing to the silver (stabilization) layer on the

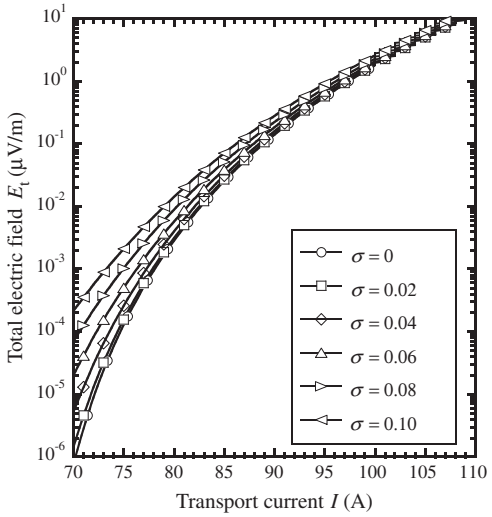

Fig. 13. Analysis results of the total electric field (E_t) of the coil (Fig. 11) for different values of the transport current (I) and standard deviation (σ). The curves are obtained as the expected values by means of Eqs. (1)–(4).

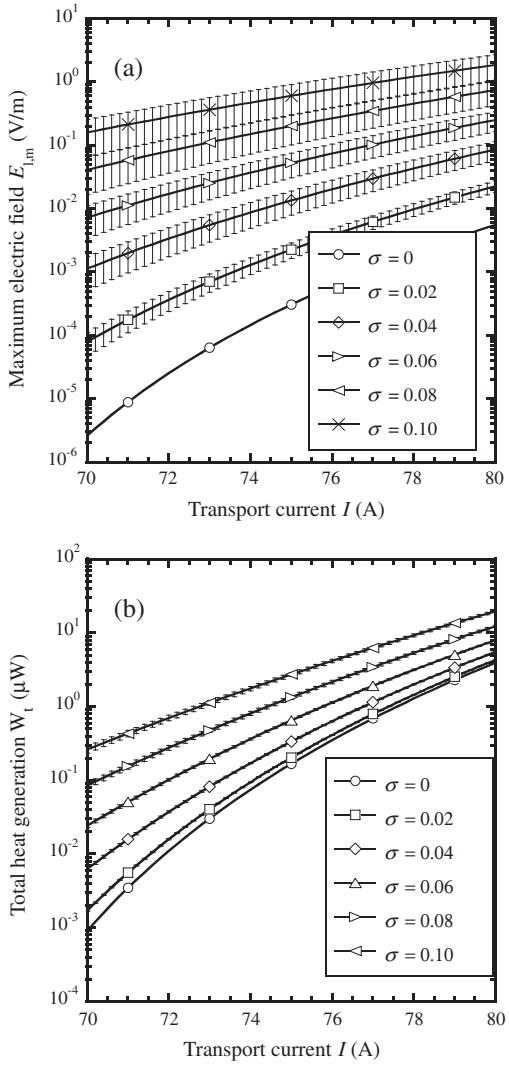

Fig. 14. Analysis results of (a) the maximum local electric field ($E_{l,m}$) and (b) the total heat generation (W_t) of the coil (Fig. 11) for different values of the transport current (I) and standard deviation (σ). The curves are obtained as the expected values by means of Eqs. (1)–(4). Error bars are also shown for the event number 100. (a) Maximum local electric field ($E_{l,m}$), (b) Total heat generation (W_t).

current transport property, especially at the higher electric field resign, and this should be clarified in our future study.

From the above results, there is a possibility that the longitudinal inhomogeneity exerts a serious as well as complex influence on the current transport properties in the system, e.g., coil structure, where the magnetic field vectors are complicatedly distributed in the system. In other words, the influences of such inhomogeneity are subject to be dependent on the actual size and/or structure of the apparatus. This means that the tolerance of the longitudinal distribution is changeable on such dependency.

Note that the recent report says the apparent critical currents largely differ depending on the distance between the electrodes for evaluation [34], and that should be clear in this study hereafter. As it is mentioned at the end of Section 1 that we concentrate on the macroscopic quantities obtained from the TapeStar™ and the four-probe method, and then we have not yet provided guidance for developments of materials. In order to make this study possible, it is necessary to relate our study to the mesoscopic evaluation method, e.g., visualization technique for the local dissipation in the tapes reported by Kiss's group [35], and then is needed to examine it in connection with the practical material production technique. This should also be our future work. In any case, if the σ is derived by the measurement of the local critical current distribution using the sample that possesses adequate periodicity of the spatial fluctuation, no matter how the statistical inhomogeneity appears along the longitudinal direction, there is a potentiality that the maximum local electric field and the total heat generation are precisely evaluated to some extent. The length for such periodicity surely depends on the manufacturing process, and then the clarification of such length will become our important work.

5. Conclusion

We have performed the statistical evaluation of the inhomogeneous current transport properties along the longitudinal direction in the GdBCO-coated conductors, for the purpose of practical realization of the high temperature superconducting system. First, the local critical current distributions obtained from the TapeStar™ (electric field criterion: approx. 1 $\mu V\,m^{-1}$; spatial resolution: approx. 0.5 mm) are summed up. By comparison of the aforementioned value with the current transport properties obtained from the four-probe method (electric field criterion: approx. 10–100 $\mu V\,m^{-1}$, spatial resolution: approx. 300–2400 mm), there exist two kinds of inhomogeneity, i.e., the statistical inhomogeneity (Gaussian distribution) and the accidental inhomogeneity along the longitudinal direction. To make the statistical inhomogeneity quantitative is likely to provide guidance for acceptable longitudinal distribution to meet the practical needs of its applied study in terms of the improvement of the tape production process. On the other hand, because the accidental inhomogeneity corresponds to so-called "yields" that makes its prediction difficult, it must be excluded as industrial materials. Furthermore, we have designed a simple pancake coil, and then the influence of the statistical inhomogeneity on the current transport properties is elucidated through the statistical evaluation. By advancing the knowledge acquired in our study, we expect that it is possible to clarify the tolerant inhomogeneity of the critical current along the longitudinal direction of the coated conductors, depending upon such applications as superconducting magnets, superconducting power transmission cables and superconducting rotor windings. By combining our method with the local dissipation evaluation technique such as Ref. [35], we will clarify the mechanism of the longitudinal inhomogeneity of the current transport properties in more detail, in order to provide the feedback information on material development.

Acknowledgements

The first author (T.N.) would like to thank Ms. Nana Okada and Mr. Katsutoku Takeuchi at the Department of Electrical Engineering, Graduate School of Engineering, Kyoto University, Japan (they graduated on March, 2011) for their support to our study. T.N. also appreciates Mrs. Sachiko Kozaki for her help to translate the original paper. This work was partly supported by the New Energy and Industrial Technology Development Organization (NEDO) as the Material and Power Applications of Coated Conductors (MPACC).

References

[1] Yagi M, Mukoyama S, Amemiya N, Ishiyama A, Wang X, Aoki Y, et al. Progress of 275 kV-3 kA YBCO HTS cable. Physica C 2011;471:1274–8.
[2] Ohya M, Yumura H, Masuda T, Amemiya N, Ishiyama A, Ohkuma T. Design and evaluation of 66 kV-class HTS power cable using REBCO wires. Physica C 2011;471:1279–82.
[3] Mizuno K, Ogata M, Nagashima K. Five tesla class YBCO magnet cooled by single stage cryocooler – Magnet fabrication and excitation test. Abstr CSJ Conf 2012;86:29 [in Japanese].
[4] Miyazaki H, Iwai S, Tosaka T, Tasaki K, Ishii Y. Development of large scale racetrack coil wound with YBCO tapes. Abstr CSSJ Conf 2012;86:130 [in Japanese].
[5] Iijima Y, Matsumoto K. High-temperature-superconductor coated conductors: technical progress in Japan. Supercond Sci Technol 2000;13:68–81.
[6] Sugano M, Nakamura T, Shikimachi K, Hirano N, Nagaya S. Stress tolerance and fracture mechanism of solder joint of YBCO coated conductor. IEEE Trans Appl Supercond 2007;17:3067–70.
[7] Cheggour N, Ekin JW, Thieme CLH, Xle YY. Effect of fatigue under transverse compressive stress on slit Y–Ba–Cu–O coated conductors. IEEE Trans Appl Supercond 2007;17:3063–6.
[8] Nagaya S, Hirano N, Watanabe T, Awaji S, Ishiyama A. A new stress control structure for high strength pancake coil wound with ReBCO conductors – Proposal of new stress control structure. Abstr CSSJ Conf 2012;86:24 [in Japanese].
[9] Manabe T, Nakamura T, Higashikawa K, Shikimachi K, Hirano N, Nagaya S. Study on heat loss characteristic of bundled MOCVD–YBCO coated conductors. Abstr CSJ Conf 2007;77:126 (in Japanese).
[10] Nagasaki Y, Nakamura T, Funaki I, Ashida Y, Yamakawa H. Thermal conduction characteristics of Bi- and Y-system tape conductors aiming at conduction-cooled magnet. TEION KOGAKU 2012;47:597–604 (in Japanese).
[11] Wilson MN. Superconducting magnets. Clarendon Press; 1983.
[12] Iwasa Y. Case studies in superconducting magnets. 2nd ed. Springer; 2009.
[13] Ishiyama A, Yanai M, Morisaka T, Ueda H, Shiohara Y, Izumi T, et al. Normal transition and propagation characteristics of YBCO tape. IEEE Trans Appl Supercond 2005;15:1659–62.
[14] Kiss T, Nakamura T, Inoue M, Takeo M, Irie F, Yamafuji K. Transport characteristics in high T_c superconductors. In: Proceedings of MT15 2, 1998: 1052–1055.
[15] Kiss T, Nakamura T, Hasegawa K, Inoue M, Okamoto H, Funaki K, Takeo M, Yamafuji K, Irie F. Nonlinear resistance in high T_c superconductors as a function of bias current density, temperature and magnetic field. In: Proceedings of ICEC17, 1998: 427–430.
[16] Kiss T, Hasegawa K, Inoue M, Takeo M, Okamoto H, Irie F. Critical current properties in high T_c superconductors. TEION KOGAKU 1999;34(7):322–31 (in Japanese).
[17] Nakamura T. Evaluation technique and applications of Bi-system HTS tape conductors. Function and Materials (CMC Publishing CO., LTD, Japan) 2004;24(2):40–9.
[18] Yamafuji K, Kiss T. A new interpretation of the glass–liquid transition of pinned fluxoid in high T_c Superconductors. Physica C 1996;258:197–212.
[19] Higashikawa K, Nakamura T, Hoshino T. Anisotropic distributions of current density and electric field in Bi-2223/Ag coil with consideration of multifilamentary structure. Physica C 2005;419:129–40.
[20] Higashikawa K, Nakamura T, Hoshino T, Muta I. Design of Bi-2223/Ag coil based on genetic algorithm and finite element method. IEEE Trans Appl Supercond 2005;15:1895–8.
[21] Higashikawa K, Nakamura T, Okamoto H. Optimal design of a Bi-2223/Ag coil for superconducting magnetic energy storage at different operating temperatures. Supercond Sci Technol 2005;18:1445–53.
[22] Higashikawa K, Nakamura T, Okamoto H. Analysis of discharging characteristics in a Bi-2223/Ag coil for SMES with consideration of cooling capacity of a cryocooler. IEEE Trans Appl Supercond 2006;16:578–81.
[23] Higashikawa K, Nakamura T, Shikimachi K, Hirano N, Nagaya S, Kiss T, et al. Conceptual design of HTS coil for SMES using YBCO coated conductor. IEEE Trans Appl Supercond 2007;17:1990–3.
[24] Higashikawa K, Nakamura T, Sugano M, Shikimachi K, Hirano N, Nagaya S. Performance improvement of YBCO coil for high-field HTS-SMES based on homogenized distribution of magnetically–mechanically influenced critical current. IEEE Trans Appl Supercond 2008;18:758–61.

[25] Higashikawa K, Kiss T, Inoue M, Imamura K, Nakamura T, Awaji S, et al. Coupled analysis method for high-field magnet coil using coated conductor based on characteristics as a function of temperature, magnetic field vector and mechanical strain. IEEE Trans Appl Supercond 2009;19:1621–5.
[26] Nakamura T, Kanzaki H, Tsuboi T, Higashikawa K, Hoshino T, Muta I. Analysis of shielding property in Bi-2223/Ag multifilamentary tapes with multi-layer arrangement. J Mater Proc Technol 2005;161(1–2):22–7.
[27] Nakamura T, Kanzaki H, Higashikawa K, Hoshino T, Muta I. Analysis of shielding layers in HTS cable taking account of spiral structure. IEEE Trans Appl Supercond 2005;15:1747–50.
[28] Nakamura T, Higashikawa K, Shikimachi K, Hirano N, Nagaya S. Influence of longitudinal inhomogeneity on current transport characteristics in Y-system HTS conductors for SMES, The Papers of Technical Meeting on Applied Superconductivity, IEE Japan 2007: 13-17 (in Japanese).
[29] Furtner S, Nemetschek R, Semerad R, Sigl G, Prusseit W. Reel-to-reel critical current measurements of coated conductors. Supercond Sci Technol 2004;17:S281–284.
[30] Nakao K, Machi T, Miyata S, Muroga T, Ibi A, Watanabe T, et al. Non-destructive characterization of long coated conductors using a Hall sensor array. Physica C 2006;445–448:669–72.
[31] Yamafuji K, Wakuda T, Kiss T. Generalized critical state model in high-T_c superconductors. Cryogenics 1997;37(8):421–30.
[32] Mawatari Y, Yamasaki H, Kosaka S, Umeda M. Critical current properties and vortex-glass-liquid-transition in Ag-sheathed Bi-2223 tapes. Cryogenics 1995;35(3):161–7.
[33] Higashikawa K, Nakamura T, Shikimachi K, Hirano N, Nagaya S. Influence of longitudinal variation of critical current in MOCVD-YBCO conductor on current transport characteristics of SMES coil. Abstr CSJ Conf 2007;76:184 (in Japanese).
[34] Cannon Jr JJ, Malozemoff AP, Diehl R, Antaya P, Mori A. Effect of length scale on critical current measurement in high temperature superconductor wires. IEEE Trans Appl Supercond 2013;23:8002005.
[35] Kiss T. Spatially resolved measurements on local current flow and vortex dynamics in superconductors. OYO BUTURI 2010;79:38–41 (in Japanese).